OPEN ACCESS

Extending the Lifetime of pH Microelectrode with Stabilized Palladium Hydride

Journal of The Electrochemical Society, 2023 **170** 087509

Extending the Lifetime of pH Microelectrode with Stabilized Palladium Hydride

Yuanjiao Li,[1] Samuel C. Perry,[2] and Janine Mauzeroll[1,z]

[1]*Department of Chemistry, McGill University, 801 Sherbrooke Street West, Montreal H3A 0B8, Quebec, Canada*
[2]*Department of Chemistry, University of Southampton, University Road, Southampton SO17 1BJ, United Kingdom*

We report a new fabrication method to produce palladium hydride pH microelectrode using a chemical approach to synthesize the palladium hydride. In contrast to electrochemically generated palladium hydride microelectrodes, chemically generated palladium hydride microelectrodes are longer lasting and importantly have a good analytical performance under aerobic conditions. Chemically generated palladium hydride microelectrodes perform best in acid to neutral electrolytes devoid of Cl^-. They can readily be produced on 10 μm diameter disk platinum microelectrodes, which makes them attractive candidates for future localized electrochemical studies.

 [DOI: 10.1149/1945-7111/acedd1]

Manuscript submitted March 3, 2023; revised manuscript received July 26, 2023. Published August 17, 2023.

Supplementary material for this article is available online

The fabrication of reliable and stable pH microsensors is an active research area for localized pH measurements in corrosion,[1–3] scanning electrochemical microscopy (SECM),[4,5] biological research,[6,7] and chemical reactions.[8,9] Various pH microsensors with potentiometric,[10–13] amperometric[14,15] or voltammetric[16–19] natures have been reported. The commonly used glass pH electrode is a potentiometric pH sensor, which measures the open circuit potential (OCP) dependent on the pH of solutions. However, it is difficult to miniaturize due to the fragile and rigid glass membrane. Non-glass materials[20–24] were explored to fabricate miniaturized pH sensors through various methods, like electrodeposition,[25,26] sputtering,[27] screen printing[28] and sol-gel.[29] Among them, metal/metal oxides have received great attention.[30] RuO_2,[31] IrO_2,[32,33] TiO_2,[34] SnO_2,[35] and the mixed oxide systems[36–38] have been widely reported because of their fast potentiometric response, and good stability. However, many challenges remain regarding the fabrication of micrometer size sensors.

A particular effort has been focused on Pd due to the capability of hydrogen absorption, forming three phases of Pd hydride (PdH_x) depending on the hydrogen content.[39] α phase has a low hydrogen content ($x < 0.017$ for PdH_x). As the H to Pd atomic ratio increases ($0.017 < x < 0.58$), a mixed $\alpha + \beta$ phase is generated. Once saturated with hydrogen, the β phase will form with a high hydrogen content of $x > 0.58$. During the phase transition, the lattice retains a face-centered cubic (fcc) structure but undergoes expansions due to the intercalation of hydrogen atoms.[40] In the pure α and β phase, the OCP of Pd hydride in a solution varies with the change of hydrogen content, while the mixed $\alpha + \beta$ phase has a constant potential regardless of the lattice hydrogen content.[41]

Taking advantage of the stable potential of $\alpha + \beta$ phase, Pd hydride has been used as reference electrodes[42,43] and pH sensors.[9,44–47] However, the application of Pd hydride pH sensor is limited by the spontaneous release of H_2 gas. To mitigate the H_2 release, Pd wires with diameters from hundreds of micrometers to millimeters were encapsulated with Teflon[45,47] and lacquer[46] to reduce the exposed surface. The masked Pd wires loaded with hydrogen in solutions can maintain the $\alpha + \beta$ phase for 12 h to 3 weeks depending on the exposed surface to volume ratio of Pd, which had been used for pH measurements in buffered fluoride etch solutions[45] and crevice corrosion.[46] However, miniaturizing Pd hydride sensors to micrometer size leads to the decrease of hydrogen storage. The consumptionof the hydrogen by dissolved oxygen will become pronounced for microsensors, resulting in phase and potential instability at the tip.[48] To increase the hydrogen storage at the tip surface, a nanostructured Pd hydride pH microelectrode was reported by electrodepositing a Pd film in the hexagonal liquid crystal template on a 25 μm diameter microelectrode.[9,44] The huge electroactive surface area extended the lifetime of pH microelectrodes to 2–3 h under deaerated conditions. However, purging the solution with inert gas changes the local pH, leading to unreliable pH measurements. In the presence of dissolved oxygen, the lifetime will significantly reduce.

To obtain a Pd pH microsensor with a high stability under aerobic conditions, a stable $\alpha + \beta$ phase is required. In 2015, Zhao and co-workers reported the synthetic method to make $PdH_{0.43}$ nanocrystals by annealing the pre-synthesized Pd nanocrystals in DMF for 16 h at 160 °C.[49] The chemically formed $PdH_{0.43}$ has a stability of 10 months under ambient conditions, which is a promising $\alpha + \beta$ phase for Pd hydride microsensors. In this work, we successfully employed the synthesized Pd hydride to produce a 10 μm diameter pH microelectrode with a lifetime of at least one month. A nanostructured Pd film was electrodeposited on the surface of a 10 μm Pt disk microelectrode and loaded with hydrogen in DMF to generate $\alpha + \beta$ phase Pd hydride. The chemically generated Pd hydride (C-PdH) microelectrode displayed a good linear potentiometric response to pH under acidic conditions, which is comparable with the electrochemically generated Pd hydride (EC-PdH) pH microelectrode. Significantly, the C-PdH microelectrode with an extended lifetime will provide a prospect of long-term localized pH measurement. Despite the imperfections as pH microsensors, the demonstration indicates the possibilities of the new Pd hydride material besides a catalyst in synthesis.[49] This could motivate the exploration of Pd hydride to overcome the release of hydrogen and provide more possibilities for its applications in other fields.

Experimental

Chemicals and materials.—Ammonium tetrachloropalladate ($(NH_4)_2PdCl_4$), 99.99%), Brij® 58 (polyethylene glycol hexadecyl ether, polyoxyethylene (20) cetyl ether), heptane (anhydrous, 99%), N,N-Dimethylformamide (DMF, 99.8%), sodium chloride (NaCl, anhydrous, 99.8%), hydrochloric acid (HCl), sulfuric acid (H_2SO_4), monosodium phosphate (NaH_2PO_4), disodium phosphate (Na_2HPO_4), Citric acid ($C_6H_8O_7$) were purchased from Sigma-Aldrich. Hydrochloric acid (HCl) was purchased from ACP. Potentials were recorded against a commercial Mercury/mercurous sulfate (SMSE) reference electrode unless otherwise specified and a Pt wire worked as the counter electrode (CE). All electrochemical measurements were conducted using the HEKA potentiostat/galvanostat (bipotentiostat model PG340, Germany).

[z]E-mail: janine.mauzeroll@mcgill.ca

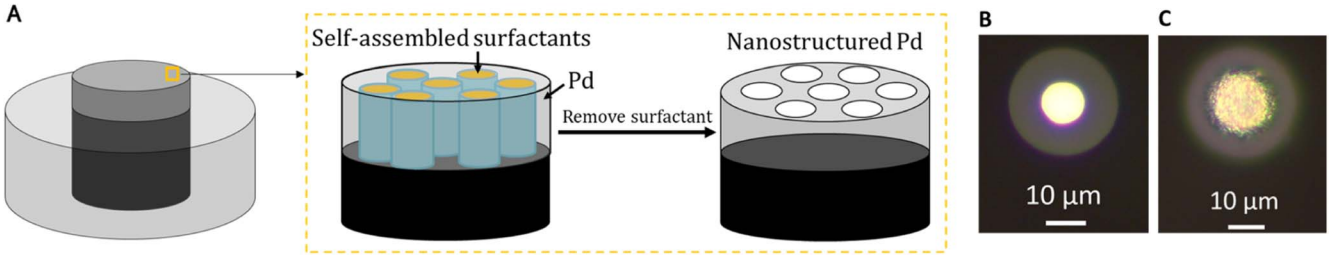

Figure 1. (A) Schematic of fabricating nanostructured Pd film on a microelectrode using true liquid crystal templating method. Optical microscopic images of the 10 μm Pt microelectrode (B) before and (C) after Pd film deposition.

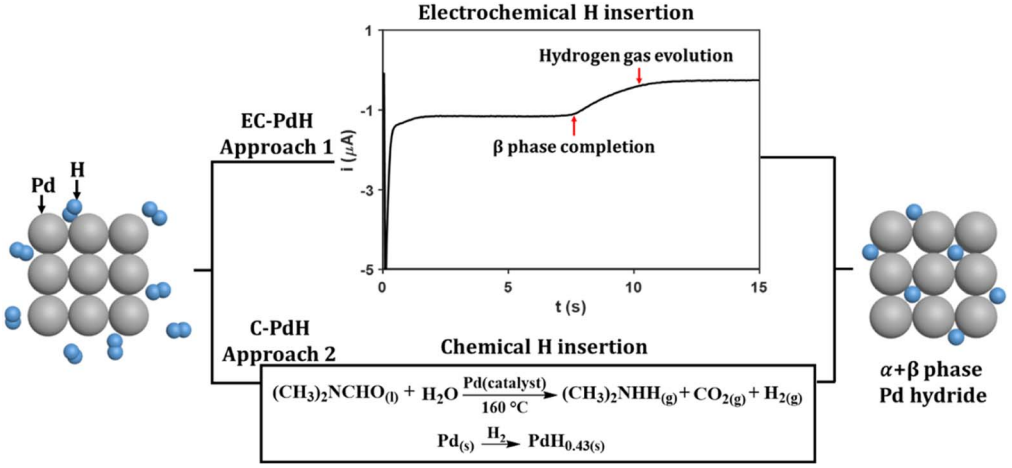

Figure 2. Pd lattice was inserted with hydrogen atoms by two approaches. In the electrochemical approach (Approach 1), −0.8 V vs SMSE was applied to produce H_2. In the chemical approach (Approach 2), Pd catalyzed DMF decomposition at 160 °C to produce H_2. The generated H_2 was absorbed by the nanostructured Pd film to produce EC-PdH and C-PdH respectively.

Fabrication of Pt microelectrodes.—The 10 μm disk microelectrodes were fabricated as previously reported.[50] Briefly, the soda-lime glass capillaries were pulled into two symmetric micropipettes using a laser-based micropipette puller (Sutter Instrument, P-2000) with a program of Heat = 240, Filament = 5, Velocity = 60, Delay = 140 and Pull = 70. A 1 cm long Pt wire with a diameter of 10 um was inserted in the pipette tip and sealed by placing the tip in a heating coil (Narishige PC-10) for 10–20 s at the maximal temperature for 3 repeats.

A Cu wire was connected to the sealed Pd wire by silver epoxy glue which was subsequently solidified at 120 °C for 15 min. After that, the assembly was inserted into a larger borosilicate capillary for additional protection. Lastly, a gold connector pin was soldered to the copper wire. All the electrodes were mechanically polished using a polishing machine (Struers, Tegrapol 23).

Electrodeposition of nanostructured Pd film.—A porous Pd film was deposited on the microelectrode according to T. Imokawa et al.[44] using the true liquid crystal templating method (Fig. 1A).[51,52] Basically, a viscous paste was prepared by mixing 12 wt% $(NH_4)_2PdCl_4$, 47 wt% Brij@ 58, 2 wt% heptane and 39 wt% water.[53] A homogenous composition was obtained by stirring the paste at 35 °C for 30 min. The Brij@58 amphiphilic surfactants (>30 wt%) self-assembled to form a liquid crystal hexagonal template,[54–56] which was stabilized by cooling in an ice bath. The 10 μm Pt microelectrode (Fig. 1B), Pt wire CE and Ag/AgCl RE were placed in the paste. A current of −25 nA was applied for 600 s (Q = 15 μC) to reduce Pd^{2+} in the confined hexagonal template forming a Pd film on the microelectrode (Fig. 1C). The Pd microelectrode (PdME) was subsequently soaked in water for 24 h to remove the surfactant template. The porous nanostructure was

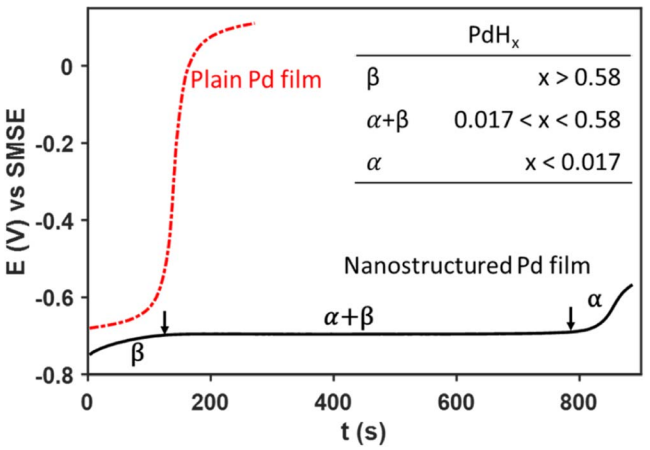

Figure 3. The phase transition of Pd hydride (the mixture $\alpha + \beta$ phase is between two arrows) for the nanostructured Pd film (black solid line) and plain Pd film (red dashed line) on the 10 μm Pt microelectrodes after electrochemical H insertion.

demonstrated in literatures by TEM.[53,57] Plain Pd film was directly electrodeposited from the 0.1 M $(NH_4)_2PdCl_4$ solution.

Electrochemically and chemically generated Pd hydride.—The intercalation of hydrogen into the Pd metallic lattice was carried out through chemical and electrochemical approaches, as illustrated in Fig. 2. For EC-PdH (Fig. 2, Approach 1),[44,58] a negative potential (−0.8 V vs SMSE) was applied to PdME in the 0.5 M Na_2SO_4 and

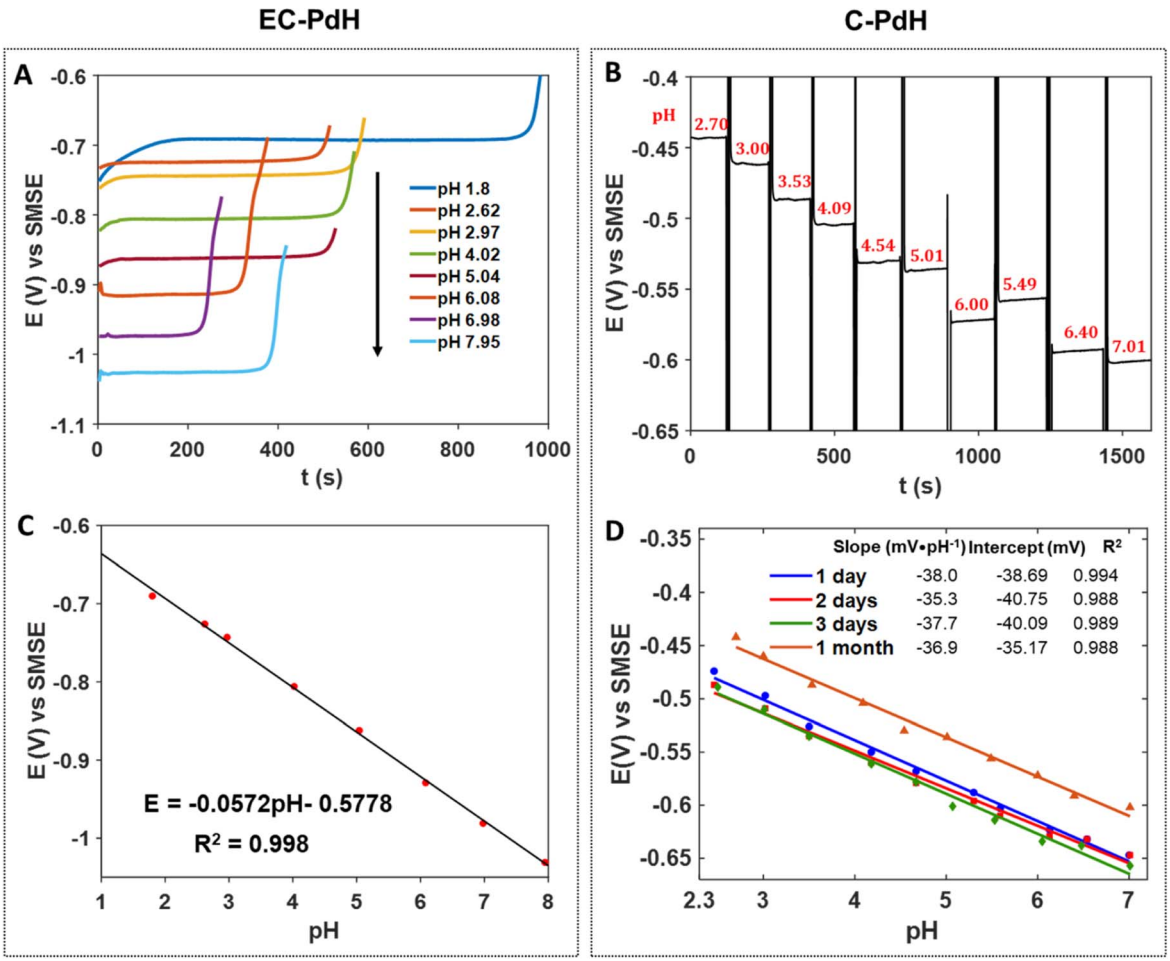

Figure 4. OCP values were monitored in different pH buffers (citric acid—Na_2HPO_4 buffers) and the corresponding calibration curves were plotted for (A, C) EC-PdH and (B, D) C-PdH. Calibration curves for the C-PdH recorded on the first day (●) when Pd film was transformed to $PdH_{0.43}$ in DMF, second day (■), third day (◆), and after one month (▶). The OCP values recorded with time after one month in different pH buffers are displayed in (B). The OCP measurements of C-PdH on the first three days are displayed in Fig. S2.

0.05 M H_2SO_4 solution (pH = 1.88) to produce H_2 which was inserted into the Pd lattice. The current decayed at ~7.5 s, representing the completion of hydrogen insertion as well as the formation of β phase Pd hydride. Once the Pd lattice was saturated, hydrogen gas evolved at 10 s reaching to a second plateau at a longer electrolysis time.

For C-PdH, hydrogen insertion into Pd lattice was implemented via the approach developed by Zhao and co-workers (Fig. 2, Approach 2).[49] The nanostructured PdME was immersed in DMF at 160 °C for 16 h in an oil bath before cooling down to room temperature. Zhao et al.[49] demonstrated the catalytic decomposition of DMF on Pd surface produced hydrogen gas, which was in turn absorbed by Pd to form Pd hydride. In the control experiments, replacing DMF with ethylene glycol and benzyl alcohol was unable to produce Pd hydride. They also proved the lattice parameter of the formed Pd hydride was larger than that of Pd using SAED, TEM and XRD and extracted the H:Pd ratio of 0.43 from XRD and XPS data, which is in the range of mixed $\alpha + \beta$ phase (H:Pd ratio, 0.017–0.58). The formed Pd hydride ME was washed by ethanol and stored in the air.

Results and Discussion

Pd nanostructure extends the lifetime of α + β phase.—To enhance the surface area, a nanostructured Pd film was electrodeposited on the microelectrode using the true liquid crystal templating (TLCT) method by the self-assembly of surfactants in a polar solvent.[51,53] At a high concentration, the surfactants form a lyotropic liquid crystal phase,[59] which can present as micellar, hexagonal, lamellar and reverse phase structures according to the critical packing parameter (CPP).[59,60] In this work, we used 47 wt% Brij@58 surfactant reported by T. Imokawa et al.[44] The surfactant molecules formed a hexagonal phase composed of cylindrical micelles as shown in Fig. 1A. Pd was electrodeposited in the aqueous domains of the hexagonal lyotropic liquid crystalline phase. Pores were left after removing the surfactant molecules, resulting in a large surface area compared with the plain Pd film. The two types of Pd films on the microelectrode were loaded with hydrogen in the 0.5 M Na_2SO_4 and 0.05 M H_2SO_4 solution via the electrochemical approach (Approach 1) as shown in Fig. 2. OCP was monitored to track the phase transition of Pd hydride. As hydrogen escaped, Pd hydride underwent three phases (Fig. 3). The potential of $\alpha + \beta$ phase was a constant value independent of the hydrogen content in the Pd lattice but responsive to the concentration of H^+ in solutions. The $\alpha + \beta$ phase of the nanostructured Pd persisted for 700 s (black solid trace in Fig. 3), whereas the duration of $\alpha + \beta$ phase of the plain film was negligible (red dashed trace in Fig. 3). This demonstrates the enhanced surface area by the porous nanostructure which allows more hydrogen atoms to be stored. Moreover, because the interior of the porous filmcan directly access the solution, Pd hydride can establish a stable equilibrium rapidly. In contrast, the plain Pd film stored a limited amount of hydrogen due to the surface saturation. Therefore, the lifetime of the nanostructured pH microelectrode can be significantly extended.

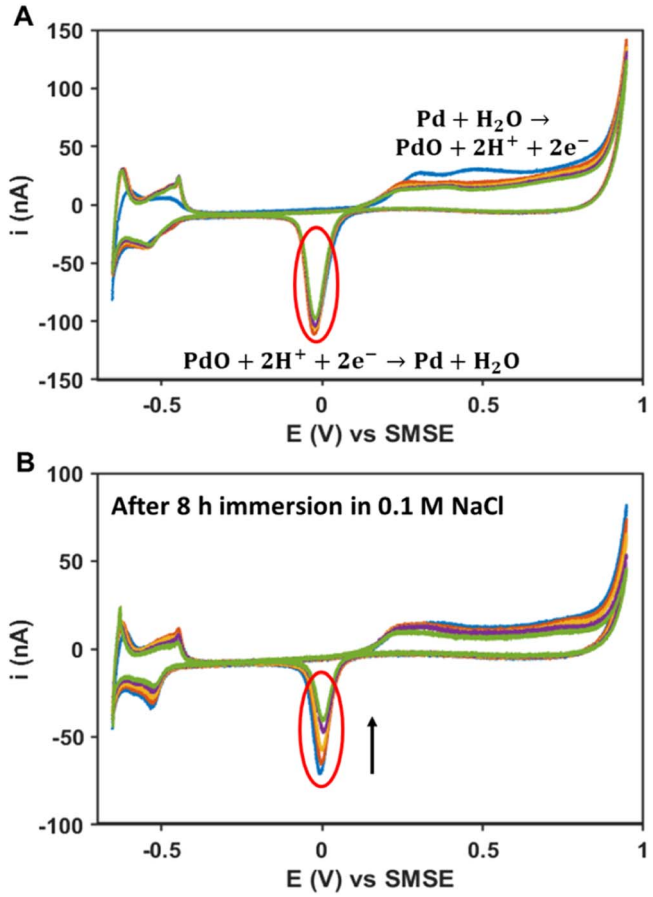

Figure 5. Cyclic voltammograms recorded in 1 M H_2SO_4 with the scan rate of 20 mVs^{-1} for the nanostructured Pd modified 10 μm Pt microelectrode (A) before and (B) after immersion in 0.1 M NaCl solution for 8 h. The peaks in red circles correspond to the reduction of Pd oxides.

Table I. The peak areas in the red circles in Fig. 5 (A) before and (B) after the 8 h immersion of the nanostructured Pd modified 10 μm Pt microelectrode in 0.1 M NaCl solution.

Cycle	Peak area (before) μC	Peak area (after) μC
1	0.362	0.188
2	0.385	0.167
3	0.353	0.135
4	0.350	0.112
5	0.343	0.089

Chemically generated Pd hydride extends the lifetime of pH microelectrode.—The calibration of the EC-PdH and C-PdH potentiometric pH microelectrodes was carried out in a series of different pH buffers. As the microelectrode was exposed to air when transferred between buffers, the release of the hydrogen would be accelerated due to oxidation, reducing the lifetime of $\alpha + \beta$ phase. Without the protection of inert gas, the lifetime of EC-PdH was several minutes, only sufficient for one buffer OCP measurement. To complete the calibration in eight buffers (Fig. 4A), hydrogen was reloaded in 0.5 Na_2SO_4 and 0.05 M H_2SO_4 solution (pH = 1.88) prior to transferring to buffer solutions. In contrast, the lifetime of C-PdH was sufficient for all buffers measurements without reloading hydrogen even after exposure to air (Fig. 4B).

The calibration curves for both EC-PdH and C-PdH displayed high linearities. C-PdH has a slope of 57.2 mV pH^{-1} (Fig. 4C),

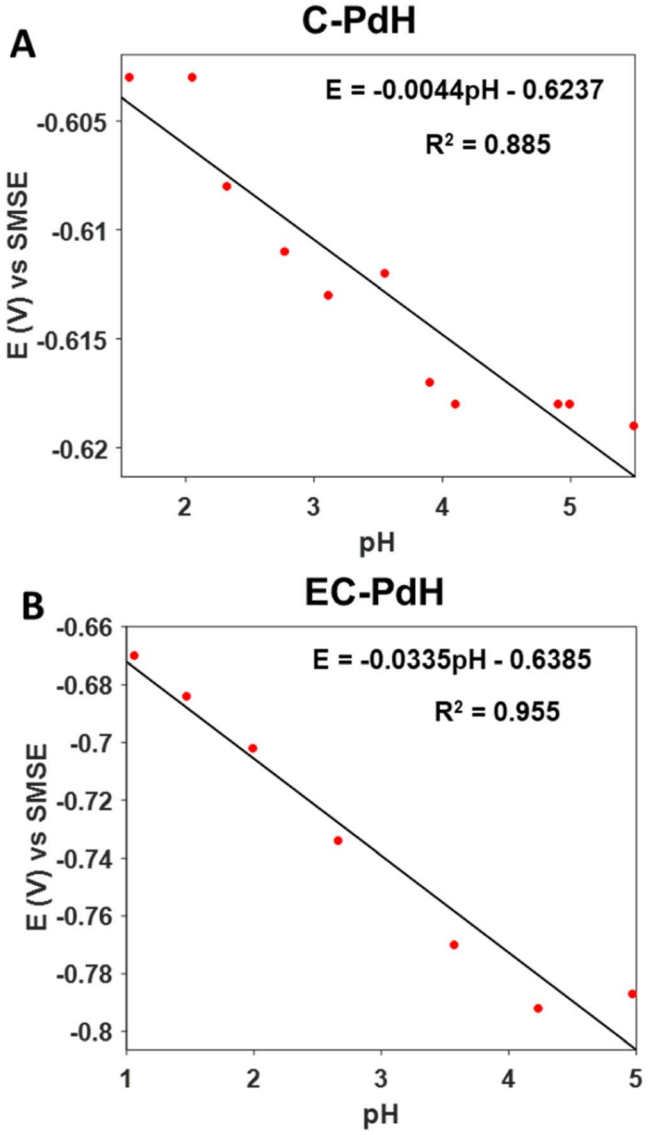

Figure 6. Calibration curves of (A) C-PdH and (B) EC-PdH in different pH H_2SO_4 solutions containing 0.1 M NaCl. OCPs were recorded vs SMSE.

which is close to the Nernstian response ($-2.303RT/F = -59.2$ mV pH^{-1} at 298 K). This is in agreement with the work by Imokawa and co-workers.[44] To extend the lifetime, they suggested to use EC-PdH under deaerated conditions. However, deaeration will complicate the measurements and disturb localized pH. By contrast, C-PdH exhibited a high stability in aerobic solutions. As shown in Fig. 4D, the calibration curves barely drifted over the first three days, which is a remarkable improvement for a 10 μm diameter Pd hydride microelectrode. Even one month later, the calibration curve remained linear. Although the intercept varied, the C-PdH microelectrode was still usable, provided a pH microsensor is usually calibrated on the day of use. The long-term stability was attributed to the passivated surface of the Pd hydride formed in DMF. Zhao et al. observed the Pd hydride transformed to Pd after introducing H_2, which could activate the passivated surface.[49] However, the potential of C-PdH became unstable in alkaline solutions (Fig. S1), reflecting the transition to α phase as hydrogen escaped. The failure in alkaline solutions could be attributed to the damage of the passivated Pd surface, which requires further studies. However, under acidic conditions, C-PdH is promising for the localized pH measurement over a long period of time.

Mechanisms of Pd hydride pH sensor.—C-PdH has an average slope of 37.0 mV pH^{-1} (Fig. 4D), which deviates from the Nernstian slope 59.2 mV pH^{-1}, implying a different pH responding mechanism from EC-PdH. The mechanism of the conventional EC-PdH pH sensor is defined by two steps. First, H atoms migrate out of the Pd lattice, generating H_2 at the electrode surface (Eq. 1). Subsequently, H_2 is involved in the redox equilibrium with aqueous protons (Eq. 2). The Nernstian slope 59.2 mV pH^{-1} resulted from the one-electron transfer in Eq. 2. Because of the continuous escape of H atoms from Pd lattice to form H_2, the partial pressure of H_2 can be assumed to be constant. The potential of Eq. 2 is thus dependent on the concentration of H^+. On the other hand, the deviated slope of C-PdH was proposed to result from the passivated Pd surface,[49] which is also the reason for the high stability. The nature of C-PdH surface and its influence on the proton redox equilibrium require further investigation.

$$Pd + \frac{x}{2}H_2 \rightleftharpoons PdH_x \quad [1]$$

$$H^+ + e^- \rightleftharpoons \frac{1}{2}H_2 \quad [2]$$

Negative effect of Cl^-.—Cl^-, Br^- and I^- were reported to mediate the shape-controlled synthesis of Pd nanoparticles, because they etch the surface of Pd.[61,62] Since Cl^--containing solutions like NaCl and KCl are the frequently used electrolytes, the effect of Cl^- on the Pd hydride pH sensors was investigated. Two opposite reactions were proposed at the Pd surface in Cl^--containing solutions. In the presence of oxygen, Pd can be oxidized to soluble $PdCl_4^{2-}$ (Eq. 3), which could be redeposited back to Pd by reductants (Eq. 4).[63,64] However, since reductants are absent in most solutions unless intentionally added, the redeposition is unlikely to occur.

$$Pd + \frac{1}{2}O_2 + 4Cl^- + H_2O \rightarrow PdCl_4^{2-} + 2OH^- \quad [3]$$

$$PdCl_4^{2-} + 2e^- \xrightarrow{\text{Reductant}} Pd + 4Cl^- \quad [4]$$

Due to the effect of Cl^-, the nanostructured Pd film deteriorated over time. The loss of Pd on the microelectrode was evaluated by cyclic voltammetry (CV) before and after immersion in 0.1 M NaCl solution for 8 h. The peaks in the red circle in Fig. 5 correspond to the reduction of surface Pd oxides that formed in the forward scan. The peak areas reflect the changes in the electroactive surface area of Pd, which were summarized in Table I. Before immersion in NaCl, the reduction peaks were consistent over five consecutive CVs. The slight decline indicates the surface damage caused by the frequent formation and stripping of Pd oxide. After 8 h immersion in NaCl solution, the peak area decreased to a larger extent in the continuous sweeps, demonstrating the Pd dissolution.

The influence of Cl^- on the pH measurement of EC-PdH and C-PdH was explored. OCPs were recorded in different pH solutions (adjusted by H_2SO_4) containing 0.1 M NaCl. The calibration slope in the presence of Cl^- decreased by 88% (Fig. 6A) and 59% (Fig. 6B) for C-PdH and EC-PdH, respectively, and the linearities worsened for both. The more severe impact on C-PdH may be because Cl^- damaged the passivated Pd surface and blocked active sites, leading to a reduction in the sensitivity. The response to Cl^- was also investigated on PdME, which showed a linear relationship between potential and log[Cl^-]. The slope and intercept changed with time (Fig. S3), implying the gradual deactivation of Pd surface by Cl^-. The damage of Cl^- to Pd suggests the use of Pd hydride electrodes should avoid Cl^- environment.

Conclusions

We report the first use of Pd hydride synthesized in DMF to make a pH microsensor. The C-PdH microelectrodes are stable for at least one month under aerobic conditions, which is a significant improvement over EC-PdH sensor performance. The new sensor response is linear in the acidic and neutral pH range and should not be used in Cl^- containing electrolytes. The excellent stability of C-PdH provides possibilities for a number of research fields with interests in the detection of localized pH changes and a new direction for the research of Pd hydride sensors. For example, this sensor fabrication method is amenable to the production of Pd hydride pH probe of small dimensions (10 μm diameter), which could be quite useful in future scanning electrochemical microscopy experiments.

ORCID

Yuanjiao Li https://orcid.org/0000-0002-3322-708X
Samuel C. Perry https://orcid.org/0000-0002-6263-6114
Janine Mauzeroll https://orcid.org/0000-0003-4752-7507

References

1. T. Kaji, T. Sekiai, I. Muto, Y. Sugawara, and N. Hara, *J. Electrochem. Soc.*, **159**, C289 (2012).
2. A. A. Panova, P. Pantano, and D. R. Walt, *Anal. Chem.*, **69**, 1635 (1997).
3. M. C. Monteiro and M. T. Koper, *Curr. Opin. Electrochem.*, **25**, 100649 (2021).
4. Y.-F. Yang and G. Denuault, *J. Chem. Soc. Faraday Trans.*, **92**, 3791 (1996).
5. D. O. Wipf, F. Ge, T. W. Spaine, and J. E. Baur, *Anal. Chem.*, **72**, 4921 (2000).
6. M. J. Marin, F. Galindo, P. Thomas, and D. A. Russell, *Angew. Chem. Int. Ed. Engl.*, **51**, 9657 (2012).
7. T. N. Bibikova, T. Jacob, I. Dahse, and S. Gilroy, *Development*, **125**, 2925 (1998).
8. N. Fomina, C. A. Johnson, A. Maruniak, S. Bahrampour, C. Lang, R. W. Davis, S. Kavusi, and H. Ahmad, *Lab Chip*, **16**, 2236 (2016).
9. M. Serrapede, G. L. Pesce, R. J. Ball, and G. Denuault, *Anal. Chem.*, **86**, 5758 (2014).
10. C. Zuliani, G. Matzeu, and D. Diamond, *Electrochim. Acta*, **132**, 292 (2014).
11. J. M. Zhang, C. J. Lin, Z. D. Feng, and Z. W. Tian, *J. Electroanal. Chem.*, **452**, 235 (1998).
12. L.-M. Kuo, Y.-C. Chou, K.-N. Chen, C.-C. Lu, and S. Chao, *Sens. Actuators B Chem.*, **193**, 687 (2014).
13. B. Lakard, O. Segut, S. Lakard, G. Herlem, and T. Gharbi, *Sens. Actuators B Chem.*, **122**, 101 (2007).
14. W. Gao and J. Song, *Electroanalysis*, **21**, 973 (2009).
15. R. Sha, K. Komori, and S. Badhulika, *IEEE Sens. J.*, **17**, 5038 (2017).
16. S. J. Cobb, Z. J. Ayres, M. E. Newton, and J. V. Macpherson, *J. Am. Chem. Soc.*, **141**, 1035 (2019).
17. K. Chaiswamongkhol, C. Batchelor-McAuley, and R. G. Compton, *Analyst*, **142**, 2828 (2017).
18. M. Amiri, E. Amali, A. Nematollahzadeh, and H. Salehniya, *Sens. Actuators B Chem.*, **228**, 53 (2016).
19. M. A. Makos, D. M. Omiatek, A. G. Ewing, and M. L. Heien, *Langmuir*, **26**, 10386 (2010).
20. D. Erne, K. Schenker, D. Ammann, E. Pretsch, and W. Simon, *Chimia*, **35**, 178 (1981).
21. J. Bobacka, A. Ivaska, and A. Lewenstam, *Chem. Rev.*, **108**, 329 (2008).
22. F. Vieira and G. Malnic, *Am. J. Physiol.*, **214**, 710 (1968).
23. W. Grubb and L. King, *Anal. Chem.*, **52**, 270 (1980).
24. D. D. Macdonald, P. R. Wentrcek, and A. Scott, *J. Electrochem. Soc.*, **127**, 1745 (1980).
25. M. Khalil, N. Liu, and R. L. Lee, *Int. J. Technol*, **9**, 447 (2018).
26. H. A. Elsen, C. F. Monson, and M. Majda, *J. Electrochem. Soc.*, **156**, F1 (2008).
27. C.-W. Pan, J.-C. Chou, T.-P. Sun, and S.-K. Hsiung, *Sens Actuators B Chem.*, **108**, 863 (2005).
28. D. K. Kampouris, R. O. Kadara, N. Jenkinson, and C. E. Banks, *Anal. Methods*, **1**, 25 (2009).
29. W.-D. Huang, H. Cao, S. Deb, M. Chiao, and J.-C. Chiao, *Sens. Actuators A Phys.*, **169**, 1 (2011).
30. L. Manjakkal, D. Szwagierczak, and R. Dahiya, *Prog. Mater Sci.*, **109**, 100635 (2020).
31. Y.-H. Liao and J.-C. Chou, *Sens. Actuators B Chem.*, **128**, 603 (2008).
32. S. Kakooei, M. C. Ismail, and B. Ari-Wahjoedi, *Int. J. Mater. Sci. Innovat*, **1**, 62 (2013).
33. F. Scarpelli, N. Godbert, A. Crispini, and I. Aiello, *Inorganics*, **10**, 115 (2022).
34. Y. Chen, S. C. Mun, and J. Kim, *IEEE Sens. J.*, **13**, 4157 (2013).
35. C.-N. Tsai, J.-C. Chou, T.-P. Sun, and S.-K. Hsiung, *IEEE Sens. J.*, **6**, 1243 (2006).
36. R. Mingels, S. Kalsi, Y. Cheong, and H. Morgan, *Sens. Actuators B*, **297**, 126779 (2019).
37. M. Pan, S. Luo, B. Yan, J. Ye, and S. Zhang, *J. Electroanal. Chem.*, **929**, 117103 (2023).
38. B. Liu and J. Zhang, *RSC Adv.*, **10**, 25952 (2020).
39. F. D. Manchester, A. San-Martin, and J. M. Pitre, *J. Phase Equilib.*, **15**, 62 (1994).

40. R. J. Wolf, M. W. Lee, R. C. Davis, P. J. Fay, and J. R. Ray, *Phys. Rev. B: Condens. Matter*, **48**, 12415 (1993).
41. M. Vasile and C. Enke, *J. Electrochem. Soc.*, **112**, 865 (1965).
42. P. Leuaa and C. Chatzichristodoulou, *J. Electrochem. Soc.*, **169**, 054534 (2022).
43. T. A. Webster and E. D. Goluch, *Lab Chip*, **12**, 5195 (2012).
44. T. Imokawa, K. J. Williams, and G. Denuault, *Anal. Chem.*, **78**, 265 (2006).
45. R. Jasinski, *J. Electrochem. Soc.*, **121**, 1579 (1974).
46. R. C. Wolfe, K. G. Weil, B. A. Shaw, and H. W. Pickering, *J. Electrochem. Soc.*, **152**, B82 (2005).
47. K. Xu, Y. Kitazumi, K. Kano, and O. Shirai, *Electrochem. Commun.*, **101**, 73 (2019).
48. M. Serrapede, G. Denuault, M. Sosna, G. L. Pesce, and R. J. Ball, *Anal. Chem.*, **85**, 8341 (2013).
49. Z. Zhao, X. Huang, M. Li, G. Wang, C. Lee, E. Zhu, X. Duan, and Y. Huang, *J. Am. Chem. Soc.*, **137**, 15672 (2015).
50. L. Danis, D. Polcari, A. Kwan, S. M. Gateman, and J. Mauzeroll, *Anal. Chem.*, **87**, 2565 (2015).
51. J. R. Bruckner, J. Bauhof, J. Gebhardt, A.-K. Beurer, Y. Traa, and F. Giesselmann, *J. Phys. Chem. B*, **125**, 3197 (2021).
52. I. Dierking and A. Martins Figueiredo Neto, *Crystals*, **10**, 604 (2020).
53. P. Bartlett, B. Gollas, S. Guerin, and J. Marwan, *Phys. Chem. Chem. Phys.*, **4**, 3835 (2002).
54. P. Van der Asdonk and P. H. Kouwer, *Chem. Soc. Rev.*, **46**, 5935 (2017).
55. G. S. Attard, J. C. Glyde, and C. G. Göltner, *Nature*, **378**, 366 (1995).
56. G. S. Attard, P. N. Bartlett, N. R. Coleman, J. M. Elliott, J. R. Owen, and J. H. Wang, *Science*, **278**, 838 (1997).
57. S. Guerin and G. S. Attard, *Electrochem. Commun.*, **3**, 544 (2001).
58. A. Rose, S. Maniguet, R. J. Mathew, C. Slater, J. Yao, and A. E. Russell, *Phys. Chem. Chem. Phys.*, **5**, 3220 (2003).
59. Y. Huang and S. Gui, *RSC Adv.*, **8**, 6978 (2018).
60. C. Fong, T. Le, and C. J. Drummond, *Chem. Soc. Rev.*, **41**, 1297 (2012).
61. N. Nalajala, A. Chakraborty, B. Bera, and M. Neergat, *Nanotechnology*, **27**, 065603 (2016).
62. M. Arenz, V. Stamenkovic, T. J. Schmidt, K. Wandelt, P. N. Ross, and N. M. Markovic, *Surf. Sci.*, **523**, 199 (2003).
63. M. Liu, Y. Zheng, L. Zhang, L. Guo, and Y. Xia, *J. Am. Chem. Soc.*, **135**, 11752 (2013).
64. Y. Xia, Y. Xiong, B. Lim, and S. E. Skrabalak, *Angew. Chem. Int. Ed. Engl.*, **48**, 60 (2009).